JACS
JOURNAL OF THE AMERICAN CHEMICAL SOCIETY
Article
pubs.acs.org/JACS

Efficient Oxidative Cycloreversion Reaction of Photochromic Dithiazolylthiazole

Takuya Nakashima, Yoshiyuki Kajiki, Sayo Fukumoto, Maki Taguchi, Satoshi Nagao, Shun Hirota, and Tsuyoshi Kawai*

Graduate School of Materials Science, Nara Institute of Science and Technology, NAIST, Ikoma, Nara 630-0192, Japan

Supporting Information

ABSTRACT: Electrochemical response of photochromic tearylenes was surveyed by means of cyclic voltammetry, DFT calculations, and spectroelectrochemistry. 4,5-Bis(2-phenyl-5-methylthiazolyl)-2-phenylthiazole was found to show electrochemical oxidative ring-cycloreversion reaction. The net current efficiency of the cycloreversion reaction under constant potential electrolysis was as high as 900%, which is ascribed to an electrochemical local-cell mechanism and a chain reaction mechanism. Electron transfer stopped-flow study using a chemical oxidant successfully identified radical cation intermediates of both closed- and open-ring isomers, involved in the oxidative cycloreversion process. The significantly long-lived radical cation of open-ring isomer with the lifetime of 33 s takes part in the indirect electron transfer process from the neutral closed-ring isomer to the radical cation of open-ring isomer in the chain reaction manner.

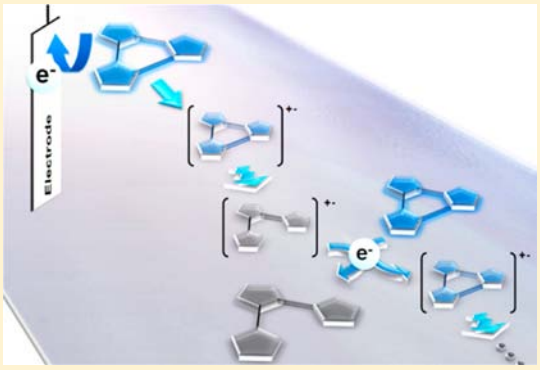

INTRODUCTION

Photoresponsive molecular materials have attracted much interest because their physicochemical properties are modulated with precise spatio and temporal control in a remote and noninvasive manner, which is required for a wide range of applications.[1−6] Photoswitching systems based on the reversible peri-cyclization reaction of hexatriene framework have been extensively studied, which is responsible for the photochromism of fulgides,[7] dihydropyrenes,[8] diarylethenes,[9] and their related compounds. Recently, we have proposed photochromic terarylenes composed of three heteroaryl groups to form a hexatriene backbone, which undergo photocyclization and cycloreversion reactions in a manner similar to diarylethenes.[10,11] A variety of combinations of aromatic groups offered the modulation of thermal bleaching of colored isomers in a wide dynamic range,[11] and photoswitching of the properties relevant to the central bridging unit including chemical reactivity,[12,13] fluorescence intensity,[14−16] and luminescent properties of metal complexes.[17,18] The precise placement of heteroatom in terarylene molecules successfully controls the molecular folding via multiple weak interactions such as CH/heteroatom, interheteroatom, and CH/π interactions in intra-[19] and intermolecular[20] manners to be in the conformation favorable for the contrarotatory cyclization reaction, leading to efficient photocyclization reaction with quantum yield above 90%. Given both the photocyclization and the -cycloreversion reactions proceed via the identical conical intersection in the potential energy surfaces, the efficiency of reactions should be dependent on the nature of conical intersection.[21,22] Therefore, it seems difficult to satisfy the high quantum yields for both the photocyclization and the -cycloreversion reactions. For instance, 2,3-dithiazolylbenzothiophene, which exhibits "photon-quantitative reaction" with cyclization quantum yield of almost unity, indeed indicates the cycloreversion reaction quantum yield smaller than 1%.[19c] Additional external stimuli such as multiphoton excitation,[23,24] heat,[25] or electric potential to trigger the cycloreversion isomerization reactions would be desirable for efficient reversible switching system. The last one is also expected to develop more complex and versatile dual-mode hybrid optical and electronic materials.[26]

Electrochemical ring-cyclization reaction was reported for hexatriene-based photochromic molecules such as fulgides[27] and dihydropyrenes.[28] Oxidative cycloreversion reaction was first reported for a closed-ring isomer of 1,2-dicyanodithienylethene.[29] Chemical modifications on the structure of diarylethenes such as the substitution of the central bridging unit with hexahydrocyclopentene ring,[30,31] the extension of π-conjugation system,[32−34] and the introduction of various substituents[30,31,35,36] have afforded diverse electrochemical responses. Electrochemical isomerization reactions also undergo with the aid of redox reactions of organometallic attached to diarylethenes as the side chain units.[37,38] The most fascinating property of electrochemical reaction is that it often involves indirect processes, which increases the net current efficiency of the reaction system.[39] For example, the electrochemically generated radical cation of closed-ring isomer spontaneously

Received: September 22, 2012
Published: November 19, 2012

   dx.doi.org/10.1021/ja309275q | J. Am. Chem. Soc. 2012, 134, 19877−19883

converts into more stable radical cation of open-ring isomer, which has enough high oxidative power to withdraw an electron from the neutral closed-ring isomer to trigger the chain reaction.[29,33]

Here, we first describe the electrochemical behavior of photochromic terarylenes (Scheme 1). Because radical

Scheme 1

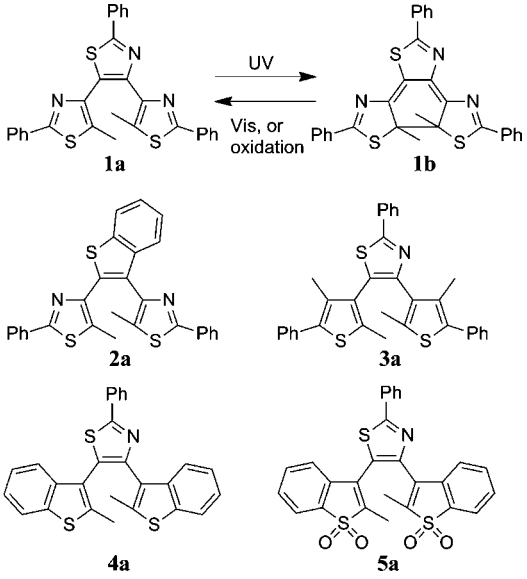

intermediates were reported to take part in the electrochemical isomerization processes, the stabilization of radical intermediates of terarylenes with three heteroaryl groups is expected to modify the electrochemical isomerization reaction. Spectroelectrochemical characterizations revealed that 4,5-bis(2-phenyl-5-methyldithiazolyl)-2-phenylthiazole (**1**) showed an oxidative cycloreversion reaction with a significantly high current efficiency. Two distinctive indirect electrochemical pathways are responsible for the enhanced efficiency. We also successfully monitored the successive evolution of both radical cation intermediates of closed- and open-ring isomers of dithiazolylthiazole with the aid of an electron transfer stopped-flow method, which provided the detailed kinetics of oxidative isomerization processes.[40]

RESULTS AND DISCUSSION

Survey of Electrochemical Properties. Electrochemical oxidative responses of open- and closed-ring isomers of terarylenes **1**−**5** were surveyed with cyclic voltammetry (CV). Terarylenes **1**−**5** possess a thiazolyl (**1a**, **3a**−**5a**) or a benzothienyl (**2a**) ring as a central bridging unit with symmetric side aromatics of phenylthiazole (**1a**, **2a**), phenylthiophene (**3a**), benzothiophene (**4a**), or dioxidized benzothiophene (**5a**). As illustrated in Figure 1, open-ring isomers of terarylenes except for **5a** with dioxidized-benzothienyl rings showed irreversible oxidation peaks above 0.9 V (vs Fc/Fc^+), which are similar to those observed for some open-ring isomers of dithienylethenes and are considered to include both the first and the second oxidation processes.[31−33] Probably due to the strong electron-accepting nature, **5a** showed no oxidation peak below 1.5 V. Meanwhile, closed-ring isomer **5b** showed an almost reversible redox couple ($E^{1/2}$ = 1.0 V). Closed-ring isomers **1b**, **2b** and **4b** gave semireversible two successive

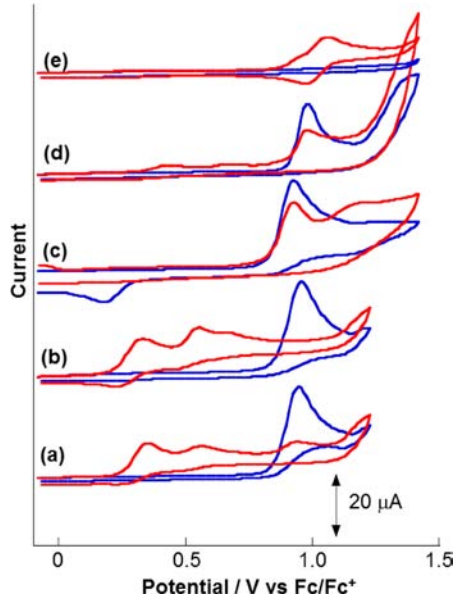

Figure 1. Cyclic voltammograms of (a) **1a** (blue) and **1b** (red); (b) **2a** (blue) and **2b** (red); (c) **3a** (blue) and **3b** (red); (d) **4a** (blue) and **4b** (red); and (e) **5a** (blue) and **5b** (red). Measurements were performed in dry acetonitrile (1×10^{-3} M) with 0.1 M of $TMAPF_6$ at a scan rate of 50 mV s^{-1}.

oxidation peaks. Especially, **1b** and **4b** showed the third oxidation peak at the same potential with those of corresponding open-ring isomers **1a** and **4a**, respectively, suggesting the formation of open-ring isomers with the electrochemical oxidation of the closed-ring isomers.

The direction of isomerization reaction subsequent to the electrochemical oxidation was deduced by the relative potential energy of oxidized forms (i.e., radical cations) of open-ring (**a**-form) and closed-ring (**b**-form) isomers calculated by the DFT method (Table 1, also see Supporting Information). The only

Table 1. Electrochemical Properties of Terarylenes, the Energy Difference of Radical Cations,[a] and Reactivity

	$E_{ox,onset}$/V vs Fc/Fc^+			
terarylenes	**a**-form	**b**-form	$\Delta E(\mathbf{a}^{\cdot+} - \mathbf{b}^{\cdot+})$/kcal mol^{-1}	subsequent reaction
1	0.89	0.24	0.168	cycloreversion
2	0.85	0.22	2.71	cycloreversion[c]
3	0.83	−0.19	5.08	−[d]
4	0.94	0.33	−2.00	cycloreversion[c]
5		0.89[b]	16.85	−[e]

[a]Total energy of radical cations in vacuum was calculated by DFT at UB3LYB/6-31+G*. [b]Reversible response was observed. [c]The reaction was not completed above 1.3 V. [d]Decomposition reactions were indicated for both **a**- and **b**-forms. [e]The formation of $\mathbf{5b}^{\cdot+}$ was indicated.

small energy differences between $\mathbf{a}^{\cdot+}$ and $\mathbf{b}^{\cdot+}$ were found for terarylenes **1**−**4**. According to the hypothesis reported by Matsuda et al.,[33] **1**, **2**, **3**, and **5** should undergo the anodic cyclization reaction, whereas **4** is possible to show the cycloreversion reaction. However, the actual directions of the anodic reactions were not accorded with those predicted based on the DFT calculation except for **4** (Table 1). In addition to the small energy differences, the solute−solvent and the ionic

dx.doi.org/10.1021/ja309275q | J. Am. Chem. Soc. 2012, 134, 19877−19883

interactions were not factored in the calculations, and therefore it was difficult to predict the direction of isomerization reaction for **1**−**4**. The anodic reaction was monitored by UV−vis absorption spectral change under varied potentials (Figures S2−S6). As summarized in Table 1, only dithiazolylthiazole **1** showed the clear subsequent cycloreversion isomerization reaction. Except for **3a**, open-ring isomers showed no significant change in absorption spectra up to 1.5 V. Closed-ring isomers **1b**, **2b**, and **4b**, which gave similar CV responses, exhibited a continuous decrease in absorption band in visible region, suggesting cycloreversion reactions. Dithienylthiazole **3** provided complex spectral changes both for open- and for closed-ring isomers, and the spectra after the electrolysis from **3a** and **3b** were different from those of **3b** and **3a**, respectively. Closed-ring isomer **5b** also showed a continuous decrease in visible band at 470 nm, while a new band appeared at 680 nm, which may correspond to the formation of radical cation of **5b**. Eventually, only dithiazolylthiazole **1** afforded a unidirectional specific subsequent reaction. We thus focus hereafter on the oxidative cycloreversion reaction of **1b** by means of electrochemical and chemical oxidation reactions.

Electrolysis of 1b. Because closed-ring isomer **1b** showed an oxidation peak at 0.35 V (vs Fc/Fc^+), the absorption spectral change was monitored under electrolysis condition at 0.42 V in acetonitrile (Figure 2). An absorption band at around 600 nm

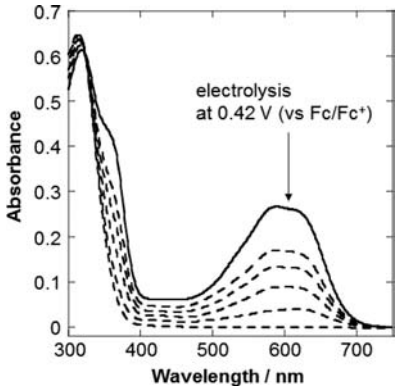

Figure 2. Change of absorption spectrum of closed-ring isomer **1b** by electrolysis at 0.42 V (vs Fc/Fc^+) in acetonitrile (2.5×10^{-4} M).

typical for closed-ring isomer **1b** continuously decreased during the electrolysis. The electrolysis reaction of **1b** was typically completed within 5 min. The absorption spectrum after electrolysis was identical to that of open-ring isomer **1a**. The spectral change with an isosbestic point at 323 nm resembles that observed for the photoinduced cycloreversion reaction from **1b** to **1a**.[11a] The final product after the electrolysis was confirmed as open-ring isomer **1a** by HPLC and ^{1}H NMR, and also showed a coloration reaction with UV irradiation to form **1b**.

We then evaluated the efficiency of electrolysis in terms of the molar amount of converted **1b** as a function of quantity of electricity during the electrolysis. The consumption of **1b** by the electrolysis was monitored by the change in absorbance at 587 nm (Figure 3a). The absorbance at 587 nm of **1b** continuously decreased and finally converged to zero after the electrolysis for 150 s, which indicates that all molecules of **1b** in the electrolysis cell were consumed and converted to **1a** by the 150 s electrolysis. Meanwhile, the current flow also decreased and reached the background after the electrolysis for 70 s; that

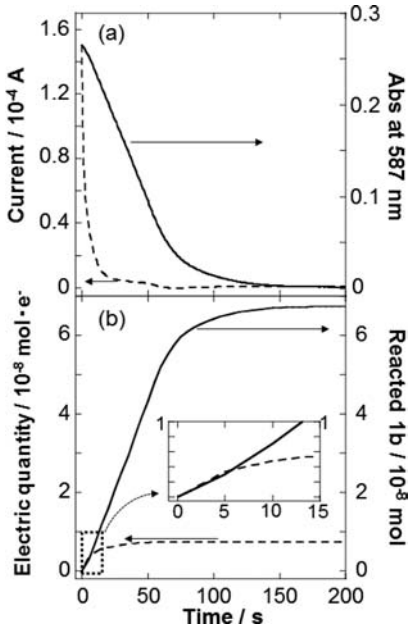

Figure 3. (a) Absorbance (at 587 nm) (−) and current (− − −) change and (b) accumulations of reacted **1b** (solid line) and quantity of electricity (broken line) as a function of time of electrolysis. Inset shows the enlarged graph of (b); *x* and *y*-axes are identical to those of (b).

is, after 70 s, the conversion reaction of **1b** did not require current injection from the working electrode, clearly demonstrating indirect processes. The current flow was converted to the quantity of electricity, which corresponds to the integral electric consumption, using the Faraday constant together with the period of electrolysis after the subtraction of background current. The electric quantity was compared to the amount of reacted **1b** (Figure 3b). Usually, 1 mol of reactant requires 1F of electricity for the quantitative electrochemical reaction with a direct process. As shown in the inset in Figure 3b, the reaction rate of **1b** almost corresponded to the electric quantity at the early stage of electrolysis within 5 s. After that, the consumption rate of **1b** was much larger than the evolution of electric quantity. Finally, the total quantity of electricity used was only 7.4×10^{-9} mol·electron, whereas the amount of reacted **1b** was 6.7×10^{-8} mol. Therefore, more than 900% of net current efficiency was recorded for the electrolysis of **1b**. The instantaneous current efficiency, which was calculated for every 5 s during the electrolysis, surprisingly reached over 2000% after 60 s (Figure S7).

The participation of indirect electrochemical processes is apparent because the decrease of absorbance at 587 nm proceeded even after the applied potential was removed (Figure S7). There would be two plausible indirect electrochemical processes responsible for such an efficient electrochemical reaction. One mechanism includes a chain reaction that takes place apart from the working electrode as already demonstrated for oxidative cycloreversion of diarylethenes (Figure 4a).[29,33] The radical cation $\mathbf{1b}^{\bullet+}$ generated by the electrode reaction of **1b** spontaneously converts to the more stable radical cation of open-ring isomer $\mathbf{1a}^{\bullet+}$. Because the ionization potential of **1a** was higher than that of **1b** as demonstrated in the CV study (Table 1) by 0.65 eV, the radical cation $\mathbf{1a}^{\bullet+}$ has enough oxidation power to oxidize another closed-ring isomer **1b** to produce $\mathbf{1b}^{\bullet+}$ without the consumption of electricity. The

dx.doi.org/10.1021/ja309275q | J. Am. Chem. Soc. 2012, 134, 19877−19883

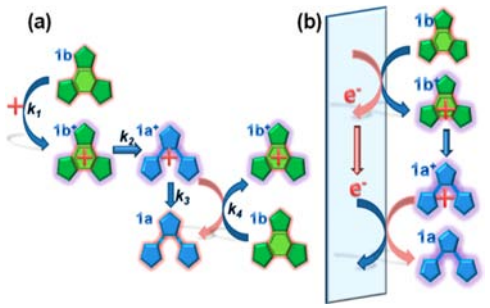

Figure 4. Two plausible indirect reaction mechanisms: (a) chain reaction model and (b) local cell reaction model.

kinetics of the spontaneous conversions of $\mathbf{1b}^{\bullet+}$ to $\mathbf{1a}^{\bullet+}$ and $\mathbf{1a}^{\bullet+}$ to **1a**, and the electron transfer from $\mathbf{1a}^{\bullet+}$ to **1b**, were studied by the stopped-flow method using a chemical oxidant, which is described later. The other reaction involves the local cell action, where the electrode mediates both anodic and cathodic reactions of substances. That is, the oxidation of **1b** and the reduction of $\mathbf{1a}^{\bullet+}$, which is formed from $\mathbf{1b}^{\bullet+}$, are coupled through the electrode. By coupling the two oxidation/reduction processes, faradaic current should be canceled, and apparently no electricity is consumed as illustrated in Figure 4b. This local cell mechanism seems rather complicated and is difficult to characterize precisely. An experiment to verify this model was demonstrated as follows (see the Supporting Information for details). The electrolysis of **1b** was conducted to accumulate the population of $\mathbf{1a}^{\bullet+}$ in a cell (cell A). This process corresponds to charging. Cell A was connected to another cell (cell B) containing an ITO (In−Sn−oxide) electrode and the same solution with cell A via a cannula filled with the electrolyte solution. The absorbance of **1b** (at 587 nm) was monitored in cell B. During the electrolysis in cell A, no absorbance change was observed in cell B. After the electrolysis in cell A for 60 s, the potential of ITO-working electrode in cell B was set to 0 V against to the ITO-electrode in cell A. Absorbance of **1b** in cell B simultaneously decreased and faradaic current was observed, which corresponds to the discharging current. The charged substance ($\mathbf{1a}^{\bullet+}$) generated in cell A during electrolysis for 60 s was consumed for the oxidation of **1b** in cell B via electrodes. In this experiment, the two working electrodes WE1 and WE2 were set at the same electrochemical potential, which is thus the model of the different parts of the same working electrode. **1b** was consumed without external current flow, indicating local cell effect. The Coulombic efficiency for this reaction as high as 150% was evaluated from the amount of consumed **1b** in cell B and faradaic electricity between WE1 and WE2.

Chemical Oxidation. The oxidative conversion of **1b** to **1a** was also studied with chemical oxidant instead of applying voltage. Tris-(*p*-bromophenyl)ammonium hexachloroantimonate ($TBPA^{\bullet+}$), which is one of stable radical ionic oxidants, was used as a chemical oxidant to trigger the oxidative cycloreversion reaction. Preliminary test by mixing of 1/10 equimolar amount of $TBPA^{\bullet+}$ to the solution of **1b** resulted in the complete bleaching of colored solution, and conversion of **1b** to **1a** was confirmed by HPLC. This cycloreversion reaction of **1b** with $TBPA^{\bullet+}$ involved neither any side reactions nor decomposition of **1**, which was confirmed by HPLC measurements after the oxidation reaction. The oxidant-based reaction yield of 1000% at the room temperature was readily observed and suggested the chain reaction mechanism.[32a] The detailed kinetics of the chemical oxidative-cycloreversion reaction was monitored by means of the stopped-flow measurements. The stopped-flow method is a useful tool to spectroscopically monitor the evolution of unstable intermediates involved in multistep reaction processes. The time resolution of electron transfer stopped-flow method was reported to correspond to high speed CV measurement with the scan rate higher than 1000 V s^{-1}.[41]

We first studied the kinetics of sequential spontaneous reactions, the conversion of $\mathbf{1b}^{\bullet+}$ to $\mathbf{1a}^{\bullet+}$ (k_2 in Figure 4a) followed by $\mathbf{1a}^{\bullet+}$ to **1a** (k_3), where the equimolar amounts of **1b** and $TBPA^{\bullet+}$ were mixed (Figure 5). As soon as both solutions

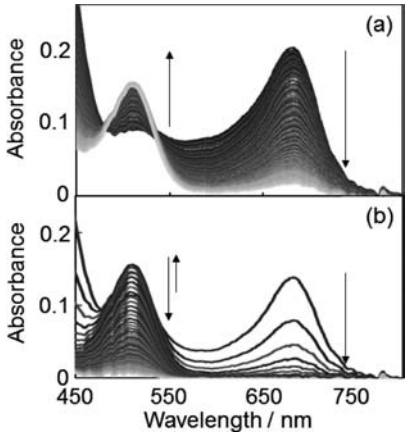

Figure 5. Stopped-flow absorption spectral change after a **1b** solution (1.2×10^{-5} M) was mixed with a $TBPA^{\bullet+}$ solution (1.2×10^{-5} M) in acetonitrile. Time intervals are 0.1 s for (a) and 2 s for (b). The recording of spectra started 5 ms after the injection of both solutions and stopped after 10 s (a) and 120 s (b).

were mixed, the strong absorption band appeared at 682 nm (Figure 5a), which was different from those of **1b** (λ_{max} = 587 nm) and $TBPA^{\bullet+}$ (λ_{max} = 708 nm). Because the difference of the oxidation potential between TBPA (0.97 V vs Fc/Fc^+) and **1b** (0.32 V vs Fc/Fc^+) was large, the electron transfer from **1b** to $TBPA^{\bullet+}$ was readily completed within the mixing time (<5 ms) to give $\mathbf{1b}^{\bullet+}$. During the waiting time of 5 ms, all neutral **1b** and $TBPA^{\bullet+}$ were consumed to produce $\mathbf{1b}^{\bullet+}$. Therefore, the oxidation reaction rate constant (k_1) of **1b** by $TBPA^{\bullet+}$ was much larger than 200 s^{-1} ($k_1 \gg 200$ s^{-1}). The absorption wavelength estimated by time-dependent DFT (TD-DFT) for $\mathbf{1b}^{\bullet+}$ (λ_{max} = 700 nm) agrees well with this experimental result (Figure S10). The decrease in the absorption band of $\mathbf{1b}^{\bullet+}$ was accompanied by the increase at 510 nm with an apparent isosbestic point (Figure 5a), which was assigned to the conversion of $\mathbf{1b}^{\bullet+}$ to $\mathbf{1a}^{\bullet+}$. Again, the TD-DFT calculation for $\mathbf{1a}^{\bullet+}$ also well reproduced the experimental absorption band. By extending the monitoring period to 120 s, the successive generation and decay processes of $\mathbf{1a}^{\bullet+}$ were recorded (Figure 5b).

The sequential reaction processes contain three components, $\mathbf{1b}^{\bullet+}$, $\mathbf{1a}^{\bullet+}$, and **1a**. The mass balance equations for these components are written as follows:

$$\frac{d[\mathbf{1b}^{\bullet+}]}{dt} = -k_2[\mathbf{1b}^{\bullet+}] \quad (1)$$

$$\frac{d[\mathbf{1a}^{\bullet+}]}{dt} = k_2[\mathbf{1b}^{\bullet+}] - k_3[\mathbf{1a}^{\bullet+}] \quad (2)$$

dx.doi.org/10.1021/ja309275q | J. Am. Chem. Soc. 2012, 134, 19877−19883

$$\frac{d[\mathbf{1}a]}{dt} = k_3[\mathbf{1a}^{\cdot+}] \quad (3)$$

These equations led to the equations for the evolutions of $\mathbf{1b}^{\cdot+}$ and $\mathbf{1a}^{\cdot+}$ as

$$[\mathbf{1b}^{+}] = [\mathbf{1b}^{+}]_0\, e^{-k_2 t} \quad (4)$$

$$[\mathbf{1a}^{\cdot+}] = [\mathbf{1b}^{+}]_0 \frac{k_2}{k_3 - k_2}(e^{-k_2 t} - e^{-k_3 t}) \quad (5)$$

where $[\mathbf{1b}^{\cdot+}]_0$ is the initial concentration of $\mathbf{1b}^{\cdot+}$, which should be equal to the concentration of **1b** injected (1.2×10^{-5} M). Because $\mathbf{1b}^{\cdot+}$ and $\mathbf{1a}^{\cdot+}$ have nonzero absorbance at 510 nm, eq 6 is regarded as

$$A\ (\text{at } 510\text{ nm}) = \varepsilon(\mathbf{1b}^{\cdot+})[\mathbf{1b}^{+}] + \varepsilon(\mathbf{1a}^{\cdot+})[\mathbf{1a}^{\cdot+}] \quad (6)$$

where $\varepsilon(\mathbf{1b}^{\cdot+})$ and $\varepsilon(\mathbf{1a}^{\cdot+})$ were molar absorption coefficients at 510 nm for $\mathbf{1b}^{\cdot+}$ and $\mathbf{1a}^{\cdot+}$, respectively. By introducing eqs 4 and 5 into 6, the temporal change of absorbance, A, at 510 nm is derived as eq 7.

$$A\ (\text{at } 510\text{ nm}) = \varepsilon(\mathbf{1b}^{\cdot+})[\mathbf{1b}^{+}]_0\, e^{-k_2 t} + \varepsilon(\mathbf{1a}^{\cdot+})[\mathbf{1b}^{+}]_0 \frac{k_2}{k_3 - k_2}(e^{-k_2 t} - e^{-k_3 t}) \quad (7)$$

The fitting curve based on eq 7 well traces the experimental data with a correlation coefficient of 0.999 with the assumed rate constants of $k_2 = (3.3 \pm 0.06) \times 10^{-1}$ s^{-1} and $k_3 = (3.0 \pm 0.009) \times 10^{-2}$ s^{-1} together with $\varepsilon(\mathbf{1b}^{\cdot+}) = 9.4 \times 10^3$ cm^{-1} M^{-1} and $\varepsilon(\mathbf{1a}^{\cdot+}) = 1.5 \times 10^4$ cm^{-1} M^{-1} as shown in Figure 6. The

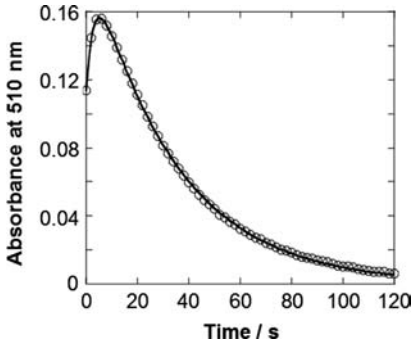

Figure 6. Temporal evolution of absorbance at 510 nm (○) reproduced from Figure 5b and the fitting curve based on eq 7 (−).

difference in the lifetimes of $\mathbf{1b}^{\cdot+}$ ($k_2^{-1} = 3$ s) and $\mathbf{1a}^{\cdot+}$ ($k_3^{-1} = 33$ s) gives rise to the apparent isosbestic points for the early stage of sequential reaction (Figure 5a). It should be also noted the surprisingly long lifetime of radical cation $\mathbf{1a}^{\cdot+}$ ($\tau = 33$ s) would be advantageous for the electron transfer in the chain reaction (Figure 4a), which would be partly responsible for the high current efficiency of the electrolysis. It also supports the results of dual-cell electrochemical experiments presented in Figures S9 and S10. Because k_3 should correspond to the reaction rate of reaction between $\mathbf{1a}^{\cdot+}$ and unknown reductant such as water, it shall be sensitive to the experimental condition such as the purity of solvents.

Finally, the kinetics of the electron transfer was studied under the condition that the chain reaction takes dominant place. The varied amounts of TBPA$^{\cdot+}$, corresponding to 2/3, 1/2, 1/3, and 1/5 equiv, were mixed with the definite quantity of **1b**. When the solutions contain neutral **1b**, the direct photoinduced cycloreversion reaction of **1b** with the rate constant of k_L by the probe light for the spectroscopy should be taken into account. We also confirmed that the radical cation state $\mathbf{1b}^{\cdot+}$ was insensitive to light irradiation. Taking the reaction rate constants (k_2–k_4) depicted in Figure 4a as well as the direct photochemical cycloreversion reaction constant k_L into account, the evolutions of all components, **1b**, $\mathbf{1b}^{\cdot+}$, $\mathbf{1a}^{\cdot+}$, and **1a**, are written as follows:

$$\frac{d[\mathbf{1b}]}{dt} = -k_4[\mathbf{1b}][\mathbf{1a}^{\cdot+}] - k_L[\mathbf{1b}] \quad (8)$$

$$\frac{d[\mathbf{1b}^{+}]}{dt} = -k_2[\mathbf{1b}^{+}] + k_4[\mathbf{1b}][\mathbf{1a}^{\cdot+}] \quad (9)$$

$$\frac{d[\mathbf{1a}^{\cdot+}]}{dt} = k_2[\mathbf{1b}^{+}] - k_3[\mathbf{1a}^{\cdot+}] - k_4[\mathbf{1b}][\mathbf{1a}^{\cdot+}] \quad (10)$$

$$\frac{d[\mathbf{1a}]}{dt} = k_3[\mathbf{1a}^{\cdot+}] + k_4[\mathbf{1b}][\mathbf{1a}^{\cdot+}] + k_L[\mathbf{1b}] \quad (11)$$

The values obtained in the previously described experiment were applied for k_2 and k_3. The rate constant of photocycloreversion reaction was separately determined in the absence of TBPA$^{\cdot+}$ to be 1.6×10^{-1} s^{-1} (Figure S11). The initial concentrations right after the mixing were zero for [**1a**] and [$\mathbf{1a}^{\cdot+}$], whereas those for [**1b**] and [$\mathbf{1b}^{\cdot+}$] were estimated from the initial values of absorbance at 510 and 587 nm, where the molar absorption coefficients for **1b** and $\mathbf{1b}^{\cdot+}$ are known. The different amount of oxidant gave different initial concentrations of [**1b**] and [$\mathbf{1b}^{\cdot+}$]. By changing the second-order rate constant k_4 as a parameter, the temporal change of concentrations of each component was simulated on the basis of eqs 8–11. As a typical example, the temporal development of each component is illustrated in Figure 7a with an assumed k_4 value of 2×10^4 s^{-1} M^{-1} for the condition of the addition 1/3

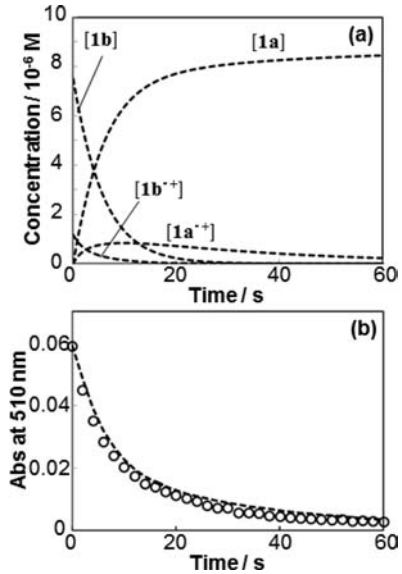

Figure 7. (a) Simulations of the evolution of each component during the cycloreversion reaction triggered by the addition of TBPA$^{\cdot+}$ (1/3 equimolar amount). (b) Temporal change of absorbance at 510 nm together with the fitting curve (broken line) reproduced using the simulated values in (a) and molar absorption coefficients for these components.

dx.doi.org/10.1021/ja309275q | J. Am. Chem. Soc. 2012, 134, 19877–19883

equimolar amount of $TBPA^{\cdot+}$. These curves reconstructed the change in absorbance at 510 nm as follows:

$$A\ (\text{at } 510\ \text{nm}) = \varepsilon(\mathbf{1b})[\mathbf{1b}] + \varepsilon(\mathbf{1b}^{+})[\mathbf{1b}^{+}] + \varepsilon(\mathbf{1a}^{\cdot+})[\mathbf{1a}^{\cdot+}] \quad (12)$$

For this reconstruction, the values of 9.4×10^3 and 1.5×10^4 cm^{-1} M^{-1} were used for $\varepsilon(\mathbf{1b}^{\cdot+})$ and $\varepsilon(\mathbf{1a}^{\cdot+})$, respectively, which were obtained from the fitting in Figure 6, and 6.4×10^3 cm^{-1} M^{-1} for $\varepsilon(\mathbf{1b})$. As shown in Figure 7b, the reconstructed curve well accorded with the experimental plot. The k_4 value of 2×10^4 s^{-1} M^{-1} reasonably reproduced the experimental results for other conditions (Figures S12–S16).

CONCLUSION

We have investigated the electrochemical response of photochromic terarylenes. 4,5-Dithiazolylthiazole **1** demonstrated highly efficient oxidative cycloreversion reaction with the net current efficiency as high as 900% and even more than 2000% provisionally. The two indirect electrochemical processes, the chain reaction and the local cell reaction mechanisms, were considered responsible for such a high current efficiency. Electron transfer stopped-flow measurements with the aid of a chemical oxidant provided the direct evidence that two radical cation intermediates were involved in the oxidative cycloreversion process; the closed-ring isomer was oxidized to radical cation, which spontaneously converted with τ = 3 s to the radical cation of open-ring isomer with a long lifetime more than 30 s. The variations of aryl units including polycyclic aromatics as well as the direction of their connections to construct a terarylene structure would give a variety of electrochemical responses including bidirectional reactions.[35b] Photo and electro dual-switching molecules that show efficient photochemical cyclization and electrochemical cycloreversion reactions would serve as a versatile material for future molecular devices.

EXPERIMENTAL SECTION

Materials and Methods. Acetonitrile (dry grade) and $TBPA^{\cdot+}$ were purchased from Wako and Aldrich, respectively, and used as received. Tetramethylammonium hexafluorophosphate ($TMAPF_6$) was purchased from Alfa Aesar and recrystallized from ethanol solution prior to use. Compounds **1**–**5** were synthesized according to the reported procedures.[11a,14,19a,c] UV–vis absorption spectra were obtained on a JASCO V-670 spectrophotometer. HPLC was performed on a HITACHI LaChrom ELITE HPLC system. Cyclic voltammetry (CV) measurements were carried out by using μ-AUTOLAB TYPE3 potentiostat/galvanostat equipped with electrochemical analysis system software. Stopped-flow measurements were conducted with a rapid-scan stopped-flow spectroscopic system (Unisoku). DFT calculations were performed with Gaussian 03[42] at B3LYP/6-31+G* for neutral compounds and at the UB3LYP/6-31+G* level for radical cations.

Electrochemical Measurements. CV measurements were conducted in a solution of 0.1 M $TMAPF_6$ in dry acetonitrile with a scan rate of 50 mV/s at room temperature in an argon-filled glovebox. A Pt disk electrode and a Pt wire were used as a working and a counter electrode, respectively. An Ag/Ag^+ electrode or an Ag wire was used as reference electrodes, which were normalized with the half-wave potential of ferrocene/ferrocenium$^+$ (Fc/Fc^+) redox couple. Typically, the concentration of dithiazolylarylenes was adjusted to be 1 mM for CV measurements. Constant potential spectro-electrochemical experiments were performed using a quartz glass cell with an indium tin oxide (ITO)-coated quartz glass plate as a working and an Ag wire as a reference electrode. A separated sample solution with a Pt wire counter electrode was connected with the quartz glass cell by a cannula, which was filled with sample solution. The applied potential was fixed to 0.42 V vs Fc/Fc^+ for electrolysis condition. The oxidative cycloreversion process was monitored by UV–vis absorption spectroscopy.

Reaction Kinetics Study. Oxidative cycloreversion reaction kinetics with an oxidant was studied at room temperature using stopped-flow measurements. The solutions of closed-ring isomer and oxidant $TBPA^{\cdot+}$ were charged to reservoirs separately and mixed in equal amounts in a reaction cell. Dynamic transformation of absorption spectra associated with the chemical reactions in the cell was recorded with the minimized time interval of 1.0 ms from 5 ms after mixing two solutions with a photodiode array detector. The temporal evolutions of absorbance at wavelength specific for reaction components were fit with reaction models to determine the rate constant of each reaction process.

ASSOCIATED CONTENT

Supporting Information

Supplementary DFT calculations, UV–vis absorption spectral change during electrolysis, experiment for indirect electrochemical processes, photoinduced cycloreversion reaction kinetics of **1b**, and stopped-flow study with varied **1b**–$TBPA^{\cdot+}$ ratios. This material is available free of charge via the Internet at http://pubs.acs.org.

AUTHOR INFORMATION

Corresponding Author

tkawai@ms.naist.jp

Notes

The authors declare no competing financial interest.

ACKNOWLEDGMENTS

This study was partly supported by NAIST, under the projects for "Bio-oriented Photoreactive Molecules" and "Green Photonics Research".

REFERENCES

(1) (a) *Molecular Switches*; Feringa, B. L., Ed.; Wiley-VCH: Weinheim, 2001.
(2) Special Issue on Photochromism: Memories and Switches. Irie, M. *Chem. Rev.* **2000**, *100*, 1683.
(3) Willner, I. *Acc. Chem. Res.* **1997**, *30*, 347–356.
(4) Yildiz, I.; Deniz, E.; Raymo, F. M. *Chem. Soc. Rev.* **2009**, *38*, 1859–1867.
(5) Stoll, R. S.; Hecht, S. *Angew. Chem., Int. Ed.* **2010**, *49*, 5054–5075.
(6) Gorostiza, P.; Isacoff, E. Y. *Science* **2008**, *322*, 395–399.
(7) Yokoyama, Y. *Chem. Rev.* **2000**, *100*, 1717–1739.
(8) Mitchell, R. H. *Eur. J. Org. Chem.* **1999**, 2695–2703.
(9) Irie, M. *Chem. Rev.* **2000**, *100*, 1685–1716.
(10) Kawai, T.; Iseda, T.; Irie, M. *Chem. Commun.* **2004**, 72–73.
(11) (a) Nakashima, T.; Atsumi, K.; Kawai, S.; Nakagawa, T.; Hasegawa, Y.; Kawai, T. *Eur. J. Org. Chem.* **2007**, 3212–3218. (b) Kawai, S.; Nakashima, T.; Atsumi, K.; Sakai, T.; Harigai, M.; Imamoto, Y.; Kamikubo, H.; Kataoka, M. *Chem. Mater.* **2007**, *19*, 3479–3483.
(12) Nakashima, T.; Goto, M.; Kawai, S.; Kawai, T. *J. Am. Chem. Soc.* **2008**, *130*, 14570–14575.
(13) (a) Neilson, B. M.; Lynch, V. M.; Bielawski, C. W. *Angew. Chem., Int. Ed.* **2011**, *50*, 10322–10326. (b) Neilson, B. M.; Bielawski, C. W. *J. Am. Chem. Soc.* **2012**, *134*, 12693–12699.
(14) Taguchi, M.; Nakagawa, T.; Nakashima, T.; Kawai, T. *J. Mater. Chem.* **2011**, *21*, 17425–17432.
(15) Suzuki, K.; Ubukata, T.; Yokoyama, Y. *Chem. Commun.* **2012**, *48*, 765–767.

(16) Pang, S. C.; Hyun, H.; Lee, S.; Jang, D.; Lee, M. J.; Kang, S. H.; Ahn, K. H. *Chem. Commun.* **2012**, *48*, 3745−3747.
(17) (a) Nakagawa, T.; Atsumi, K.; Nakashima, T.; Hasegawa, Y.; Kawai, T. *Chem. Lett.* **2007**, *36*, 372−373. (b) Nakagawa, T.; Hasegawa, Y.; Kawai, T. *J. Phys. Chem. A* **2008**, *112*, 5096−5103.
(18) Yam, V. W. W.; Lee, J. K. W.; Ko, C. C.; Zhu, N. Y. *J. Am. Chem. Soc.* **2009**, *131*, 912−913.
(19) (a) Kawai, S.; Nakashima, T.; Kutsunugi, Y.; Nakagawa, H.; Nakano., H.; Kawai, T. *J. Mater. Chem.* **2009**, *19*, 3606−3611. (b) Morinaka, K.; Ubukata, T.; Yokoyama, Y. *Org. Lett.* **2009**, *11*, 3890−3893. (c) Fukumoto, S.; Nakashima, T.; Kawai, T. *Angew. Chem., Int. Ed.* **2011**, *50*, 1565−1568.
(20) (a) Nakashima, T.; Fujii, R.; Kawai, T. *Chem.-Eur. J.* **2011**, *17*, 10951−10957. (b) Wu, Y.; Chen, S. J.; Yang, Y. H.; Zhang, Q.; Xie, Y. S.; Tian, H.; Zhu, W. H. *Chem. Commun.* **2012**, *48*, 528−530.
(21) Boggio-Pasqua, M.; Ravaglia, M.; Bearpark, M. J.; Garavelli, M.; Robb, M. A. *J. Phys. Chem. A* **2003**, *107*, 11139−11152.
(22) Ishibashi, Y.; Umesato, T.; Kobatake, S.; Irie, M.; Miyasaka, H. *J. Phys. Chem. C* **2012**, *116*, 4862−4869.
(23) (a) Miyasaka, H.; Murakami, M.; Itaya, A.; Guillaumont, D.; Nakamura, S.; Irie, M. *J. Am. Chem. Soc.* **2001**, *123*, 753−754. (b) Murakami, M.; Miyasaka, H.; Okada, T.; Kobatake, S.; Irie, M. *J. Am. Chem. Soc.* **2004**, *126*, 14764−14772.
(24) Tsuboi, Y.; Shimizu, R.; Shoji, T.; Kitamura, N. *J. Am. Chem. Soc.* **2009**, *131*, 12623−12627.
(25) (a) Kobatake, S.; Yamashita, I. *Tetrahedron* **2008**, *64*, 7611−7618. (b) Morimitsu, K.; Shibata, K.; Kobatake, S.; Irie, M. *J. Org. Chem.* **2002**, *67*, 4574−4578.
(26) Mialane, P.; Zhang, G. J.; Mbomekalle, I. M.; Yu, P.; Compain, J. D.; Dolbecq, A.; Marrot, J.; Secheresse, F.; Keita, B.; Nadjo, L. *Chem.-Eur. J.* **2010**, *16*, 5572−5576.
(27) Fox, M. A.; Hurst, J. R. *J. Am. Chem. Soc.* **1984**, *106*, 7626−7627.
(28) Mitchell, R. H.; Brkic, Z.; Sauro, V. A.; Berg, D. J. *J. Am. Chem. Soc.* **2003**, *125*, 7581−7585.
(29) (a) Koshido, T.; Kawai, T.; Yoshino, K. *J. Phys. Chem.* **1995**, *99*, 6110−6114. (b) Koshido, T.; Kawai, T.; Yoshino, K. *Chem. Express* **1993**, *8*, 553−556.
(30) (a) Browne, W. R.; de Jong, J. J. D.; Kudernac, T.; Walko, M.; Lucas, L. N.; Uchida, K.; van Esch, J. H.; Feringa, B. L. *Chem.-Eur. J.* **2005**, *11*, 6414−6429. (b) Browne, W. R.; de Jong, J. J. D.; Kudernac, T.; Walko, M.; Lucas, L. N.; Uchida, K.; van Esch, J. H.; Feringa, B. L. *Chem.-Eur. J.* **2005**, *11*, 6430−6441.
(31) Guirado, G.; Coudret, C.; Hliwa, M.; Launay, J. P. *J. Phys. Chem. B* **2005**, *109*, 17445−17459.
(32) (a) Peters, A.; Branda, N. R. *J. Am. Chem. Soc.* **2003**, *125*, 3404−3405. (b) Peters, A.; Branda, N. R. *Chem. Commun.* **2003**, 954−955.
(33) Moriyama, Y.; Matsuda, K.; Tanifuji, N.; Irie, S.; Irie, M. *Org. Lett.* **2005**, *7*, 3315−3318.
(34) Staykov, A.; Areephong, J.; Browne, W. R.; Feringa, B.; Yoshizawa, K. *ACS Nano* **2011**, *5*, 1165−1178.
(35) (a) Gorodetsky, B.; Samachetty, H. D.; Donkers, R. L.; Workentin, M. S.; Branda, N. R. *Angew. Chem., Int. Ed.* **2004**, *43*, 2812−2815. (b) Gorodetsky, B.; Branda, N. R. *Adv. Funct. Mater.* **2007**, *17*, 786−796. (c) Léaustic, A.; Anxolabéhère-Mallart, E.; Maurel, F.; Midelton, S.; Guillot, R.; Métivier, R.; Nakatani, K.; Yu, P. *Chem.-Eur. J.* **2011**, *17*, 2246−2255.
(36) Lee, S.; You, Y.; Ohkubo, K.; Fukuzumi, S.; Nam, W. *Org. Lett.* **2012**, *14*, 2238−2241.
(37) Guirado, G.; Coudret, C.; Launay, J. P. *J. Phys. Chem. C* **2007**, *111*, 2770−2776.
(38) (a) Tanaka, Y.; Ishisaka, T.; Inagaki, A.; Koike, T.; Lapinte, C.; Akita, M. *Chem.-Eur. J.* **2010**, *16*, 4762−4776. (b) Akita, M. *Organometallics* **2011**, *30*, 43−51.
(39) Andrieux, C. P.; Hapiot, P.; Saveant, J. M. *Chem. Rev.* **1990**, *90*, 723−738.
(40) Oyama, M.; Higuchi, T.; Okazaki, S. *Electrochem. Commun.* **2000**, *2*, 675−678.
(41) Oyama, M.; Matsui, J.; Park, H. *Chem. Commun.* **2002**, 604−605.
(42) *Gaussian 03*, revision D.01; Gaussian, Inc.: Wallingford, CT, 2004.